LA-UR -92-792

LA-UR--92-792

DE92 011371

Los Alamos National Laboratory is operated by the University of California for the United States Department of Energy under contract W-7405-ENG-36

TITLE X-RAY STREAK CAMERA DIAGNOSTICS OF PICOSECOND LASER-PLASMA INTERACTIONS

AUTHOR(S) J. A. Cobble
R. D. Fulton
L. A. Jones
G. A. Kyrala
G. T. Schappert
A. J. Taylor
E. K. Wahlin

SUBMITTED TO 9th Topical Conference on High-Temperature Plasma Diagnostics, Santa Fe, NM
March 15-19, 1992

DISCLAIMER

MASTER

Los Alamos Los Alamos National Laboratory
Los Alamos, New Mexico 87545

X-ray streak camera diagnostics of picosecond laser-plasma interactions

J. A. Cobble, R. D. Fulton, L. A. Jones, G. A. Kyrala,
G. T. Schappert, A. J. Taylor, E. K. Wahlin

Review of Scientific Instruments:
Proceedings of 9th Topical Conference on
High Temperature Plasma Diagnostics

Santa Fe, NM
March 16-19, 1992

Abstract

An x-ray streak camera is used to diagnose a laser-produced Al plasma with time resolution of ~10 ps. A streak record of filtered emission and a time-integrated transmission grating spectrum reveal that the plasma radiation is dominated by emission from He- and H-like resonance lines.

The diagnosis of plasmas with temporal durations of picoseconds and spatial extents of a few microns is difficult. The physicist is in this arena when a high intensity laser is focused on a solid target.[1,2,3,4] The ultimate goal is to interpret how the laser light couples to the plasma, how the radiation escapes, and how the plasma decays. Then we will understand how to enhance the absorption of the laser and to increase the x-ray yield both in energy and power. This paper discusses analysis of the temporal aspects of such an experiment with an x-ray streak camera[5,6] and shows how this diagnostic helps us reach the goal.

The laser system[7] is based on the amplification of a subpicosecond, frequency-doubled dye laser pulse at 308 nm in XeCl. An Al target is exposed to ~100 mJ in 300 fs; the irradiance on target is > 5 x 10^{18} W/cm^2. The target also sees ~ 1 mJ of prelase from amplified spontaneous emission (ASE).[8] The beam energy and the level of ASE per pulse is monitored on each shot. The ASE irradiance is in the range of mid 10^{11} W/cm^2. Thus, the main beam interacts with a preformed plasma rather than with solid material.

The diagnostic set besides the streak tube consists of an array of filtered, x-ray p-i-n diodes, a 5-μm pinhole camera, a pentaerythritol (PET) crystal spectrograph, a variable-spaced grazing incidence grating spectrometer, a micro-channel-plate grazing-incidence spectrometer, and an ion time-of-flight spectrometer. The streak camera, an unmodified Kentech x-ray device, is used in two modes. In sweep mode, we use it to streak plasma radiation filtered by five separate thicknesses of Be: 0, 28, 53, 81, and 107 μm. We discuss below what this tells about the plasma emission. The camera is also used in static mode with a free-standing Au-foil transmission grating (TGS)[9] to obtain time-integrated spectra with 0.2-

nm resolution from .4 - 10 nm (i.e., 0.1 - 3 keV). Unfortunately, the signal level is too low to streak the TGS.

These instruments enable us to get data from a single laser shot. In brief, we find[1] a plasma plume, which in ~30 ps expands to a diameter of ~10 μm and to a length of ~30 μm . The plasma electron density, which changes considerably in this time, is in the range 10^{21} - 10^{22} cm^{-3}. The mean ion charge state is between 11 and 12. The electron temperature is 1 - 3 keV. Incident laser energy is converted to He- and H-like line emission with an efficiency approaching 1%. Most of this line emission is in the 2-1 transitions.

The radiation has been examined through the Be filter pack with the streak camera. The camera photocathode is ~0.1 μm of KI deposited on 0.03 μm of Al on a nominal 0.3-μm polypropylene film. It is sensitive to soft x rays in the range 0.1 - 15 keV. It is found to respond also to 308-nm light, which is used to determine its temporal calibration.

For this calibration, laser light is put directly on the photocathode with half the streak tube slit covered with a retarder material. Using the group velocity through the retarder, we calculate the time delay which has been measured with the camera. In this way, the sweep speed is found to be 12±1 ps/mm at all positions along the 40-mm face of the image intensifier behind the camera. Because the laser light is subpicosecond, the instrument function of the streak tube at 308 nm is determined to be 4 ps at full width half maximum. X-ray signals do not permit a clean measure of the x-ray instrument function. We estimate the x-ray resolution to be 8-10 ps.

The energy response function of the photocathode, the quantum efficiency in electrons per photon R(E), is modeled as proportional to the photon energy E and its absorption coefficient μ(E).[10] For an insulating photocathode, this is modified by the limited mean free path of secondary electrons in the material, which is typically less than the x-ray mean free path. The correction is the transmission T of x rays to the back surface. Thus, $R(E) \sim \mu(E)\, E\, T(E)$. This represents all the energy-dependent terms in the response.

A contour plot of a typical streak is shown in Fig. 1. Note that the signal is in the photon counting regime so that Poisson statistics and intensifier pulse height distributions reduce the signal-to-noise ratio. Lineouts of the zones show that within the noise of the streaks, all the non-zero-thickness zones of the filter have the same duration. Even the unfiltered zone in some cases appears to have the same full-width-at-half-maximum duration: 30-40 ps. See Fig. 2. Consider three ranges of radiative energy: Li-like and lower charged ions emitting at ≤ 250 eV, He- and H-like ions emitting from 1.6-2.0 keV, and high energy bremsstrahlung ≥ 10 keV. Higher energy radiation is expected to extinguish faster. For the Li-like ions a lower excitation temperature is required, and they should radiate longer than the He- and H-like ions. The ≥ 10-keV electrons escape from the plasma in less than 1 ps; thus, the high energy bremsstrahlung cannot endure. X rays generated at the wall will be outside the field of view of the camera. The equality of zone durations suggests that the plasma radiation falls mainly into the quasi-

monochromatic 1.6-2.0-keV band. At the time of peak signal, a lineout is taken and averaged over the zones. The average over the unfiltered zone is normalized to unity so that the lineout now shows the transmissions of the spectrum through the various zones. Figure 3 show the zone-averaged result plotted on the theoretical transmissions of the zones calculated as functions of energy. The error bars on the data represent one standard deviation from the means of the zone averaging. The experimental data are plotted at 1.7 keV near the spectral centroid suggested by crystal spectroscopy. Table 1 shows the statistics of one shot and the averages over several shots. Two possible explanations for the discrepancy with zone 1 are given: (1) The 28-μm filter may be thicker. To reconcile the data, it would have to be about half again as thick. This is not a high probability error. Also since the zone 1 foil is common to all the other filtered zones, this would affect to a lesser extent their transmissions too. (2) The unfiltered channel may include some lower energy radiation which appears in none

Table 1. Statistics of the zones -- mean transmission and standard deviation: $\mu\pm\sigma$

Zone	1	2	3	4
thickness(μm)	28	53	81	107
$\mu\pm\sigma$ for several shots	.32±.03	.25±.05	.11±.03	.06±.03
$\mu\pm\sigma$ for a single shot	.34±.10	.23±.07	.11±.05	.09±.04

of the other channels. In this case, the curves in Fig. 3 are, instead of the transmission, the ratios of the n^{th} zone signals to the zeroth channel:

$$S(n)/S(0) = F_L R_L T_L(n) /[F_L R_L + F_s R_s]$$

where the subscript L refers to the line radiation at 1.6-2.0 keV and the s to the softer Li- and Be-like radiation. $T_L(n)$ is the n^{th} zone filter transmission of the radiation. F_L and F_s are the photon fluxes. In the limit as F_s approaches zero, the ratio is the plotted transmissions. The correction to the theoretical curve, which lowers them, is thus:

$$[1 + (F_s R_s /F_L R_L)]^{-1} = [1 + .38 F_s /F_L)^{-1}$$

where the .38 is the estimated ratio of the responses at .25 and 1.7 keV from the theoretical model. Were the ratio of photon fluxes equal, the correction is a 27% lowering of the curves, which would yield a reasonable fit. This is shown with the dashed lines in Fig. 3. In this event, the relative energy content of the softer radiation would be ~1/7 of the of the higher energy component.

A time-integrated TGS spectrum is illustrated in Fig. 4. For this data, the streak tube was used as a position sensitive detector. The spectrum is corrected for photocathode sensitivity as was indicated above,

for the theoretical grating efficiency[11], and for the response of the film used with the intensifier. With the TGS, Li- and Be-like emission is indistinguishable from the noise. In view of the uncertainties in both the data and the system response, it is fair to conclude that the lower charge states as seen both in the streak mode and with the TGS contribute no more than ~ 5% of the He- and H-like line energy radiated by the plasma. Note that if superthermal x rays are present, they add equally to the numerator and denominator of the ratios, which causes them to rise with respect to the experimental data. This phenomenon cannot be used to explain the quality of the fit in Fig. 3. Also, it could be argued that soft ultraviolet emission accounts for the extra signal in the unfiltered channel rather than 250-eV x rays. The reply to this is that the transmission of the photocathode approaches zero in this regime (Its response to 308 nm is believed to be a two photon phenomenon, and a high intensity is required.), and, as noted earlier, the time history of the unfiltered channel shows little evidence of a cool, UV-emitting plasma at later tines. Therefore, it is reasonable to ignore such an emission.

A second normalization can be made by taking the ratios of the Be channels to the 28-μm zone. No soft radiation is transmitted by any of these channels, but even the 107-μm zone transmits 85% at 4 keV. Thus, we can check the amount of bremsstrahlung from ~ 3-15 keV where the photocathode is fading. While the results of this exercise are not entirely consistent, we find that within the errors bars (Table 1), the continuum energy is somewhat less than the line radiation. Two relatively thick filters are not transmitting much signal. Refer once more to the TGS spectrum in Fig. 4. The existence of a high energy distribution requires an extension of the above analysis for estimating the soft radiation. Unless the flux of line radiation is considerably greater than the flux of bremsstrahlung, the relative flux of soft radiation has to increase. As noted before, the TGS spectrum indicates no such thing. The conclusion then is that based on the Kentech measurements, the intensity spectrum is $\geq 2/3$ line radiation from the He- and H-like Al with the Li- and Be-like ions adding another 5% of that. The hard radiation is likely to contribute $\leq 1/3$. Clearly, there is a need for more measurements to reduce the uncertainty here.

The utility of the streak tube in understanding the plasma is well demonstrated by using its data with pinhole camera and crystal data. As has been seen, energy approaching 1 mJ is emitted by He- and H-like line radiation in 30 ps from the surface of a cylindrical plume. The estimated line irradiance is ~ 3 TW/cm^2 at the plasma. Our next experiment will look at ways to improve these values by altering target material, surface finish, and ASE prelase.

The authors acknowledge the contributions of K. A. Stetler, J. K. Studebaker, and J. P. Roberts to this effort. This work was done under the auspices of the United States Department of Energy.

References

1. G. A. Kyrala, R. D. Fulton, E. K. Wahlin, L. A. Jones, G. T. Schappert, J. A. Cobble, A. J. Taylor, to be published in Appl. Phys. Lett., winter, 1992
2. A. Zigler, V. L. Jacobs, D. A. Newman, P. G. Burkhalter, D. J. Nagel, T. S. Luk, A. McPherson, K. Boyer, C. K. Rhodes, Phys. Rev. A **45**, 1569 (1992)
3. J. Edwards, V. Barrows, O. Willi, S. J. Rose, Appl. Phys. Lett. **57**, 2086 (1990)
4. M. Chaker, J. C. Kieffer, J. P. Matte, H. Pépin, P. Audebert, P. Maine, D. Strickland, P. Bado, G. Mourou, Phys. Fluids **B3**, 167, 1991
5. J. A. Cobble, G. A. Kyrala, A. A. Hauer, A. J. Taylor, C. C. Gomez, N. D. Delamater, G. T. Schappert, Phys. Rev. A 39, 454 (1989)
6. M. M. Murnane, H. C. Kapteyn, R. W. Falcone, Phys. Rev. Lett. **62**, 155, 1989
7. A. J. Taylor, C. R. Tallman, J. P. Roberts, C. S. Lester, T. R. Gosnell, P. H. Y. Lee, G. A. Kyrala, Optics Lett. **15**, 39 (1990)
8. J. A. Cobble, G. T. Schappert, L. A. Jones, A. J. Taylor, G. A. Kyrala, R. D. Fulton, J. Appl. Phys. **69**, 3369 (1991)
9. The 0.2-μm-period grating is manufactured by M. L. Schattenburg.
10. B. L. Henke, J. P. Knauer, K. Premaratne, J. Appl. Phys. **52**, 1509 (1981)
11. M. L. Schattenburg, **Astronomical X-Ray Spectroscopy: Studies of the Crab Nebula and Development of Ultra-fine Transmission Gratings**, MIT thesis, 1984.

Figure Captions

Fig. 1 A contour plot of the x-ray streak. The unfiltered zone is at the bottom. The 28-μm zone extends from 2-13 mm, the 81-μm zone from 13-17 mm, the 53-μm zone from 17-22 mm, and the 107-μm zone from 22 to the top.

Fig. 2 Lineouts of the streaked zones. From top to bottom, the order is the unfiltered, the 28-μm, the 53-μm, the 81-μm, and the 107-μm zone.

Fig. 3 Zone transmissions. The solid lines are the theoretical transmissions. The experimental points have one sigma error bars. The dashed lines represent the theoretical ratio of zone signals assuming equal photon flux of soft radiation.

Fig. 4 A time-integrated transmission grating spectrum.

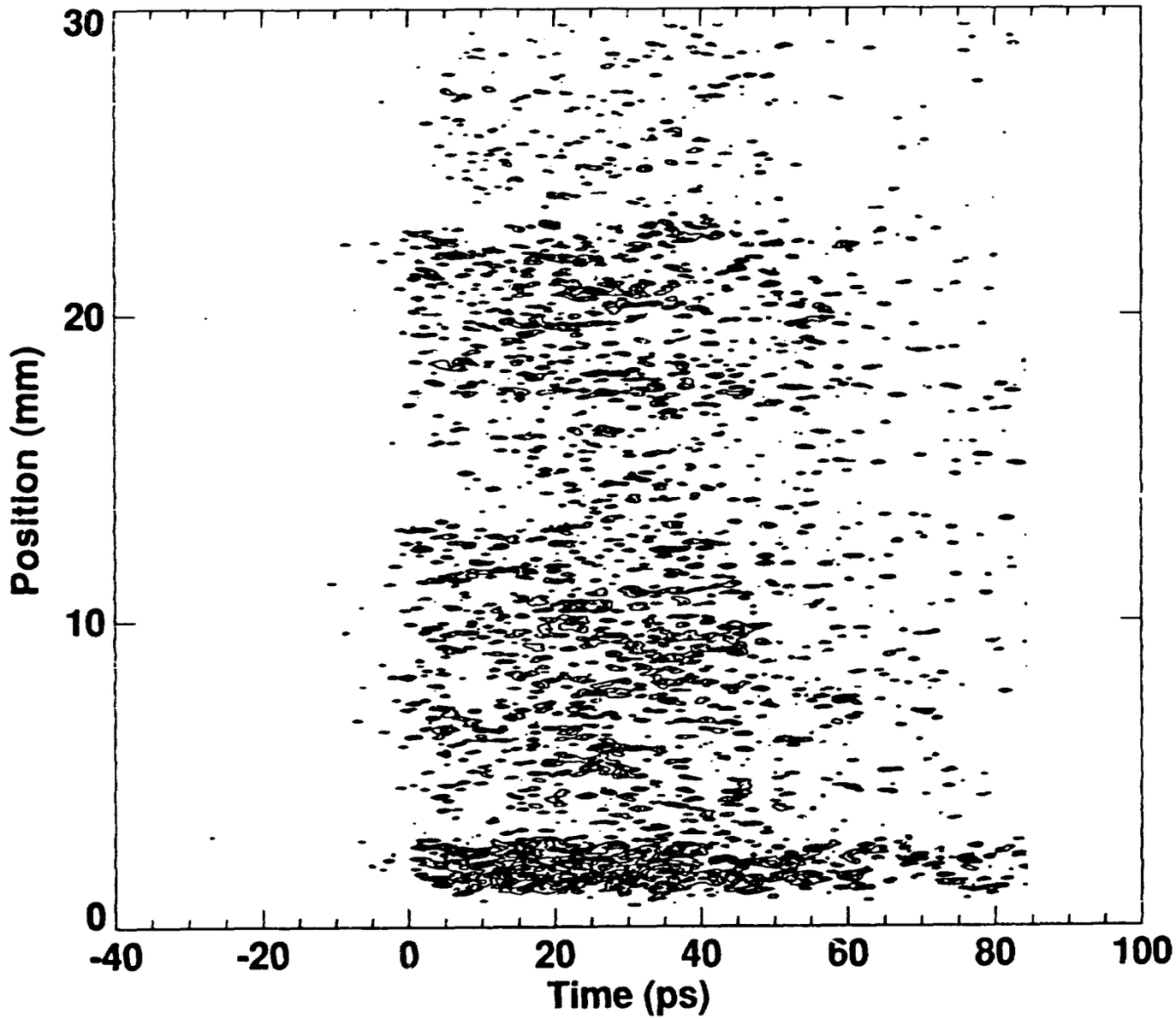
30
20
10
0
Position (mm)
-40
-20
0
20
40
60
80
100
Time (ps)

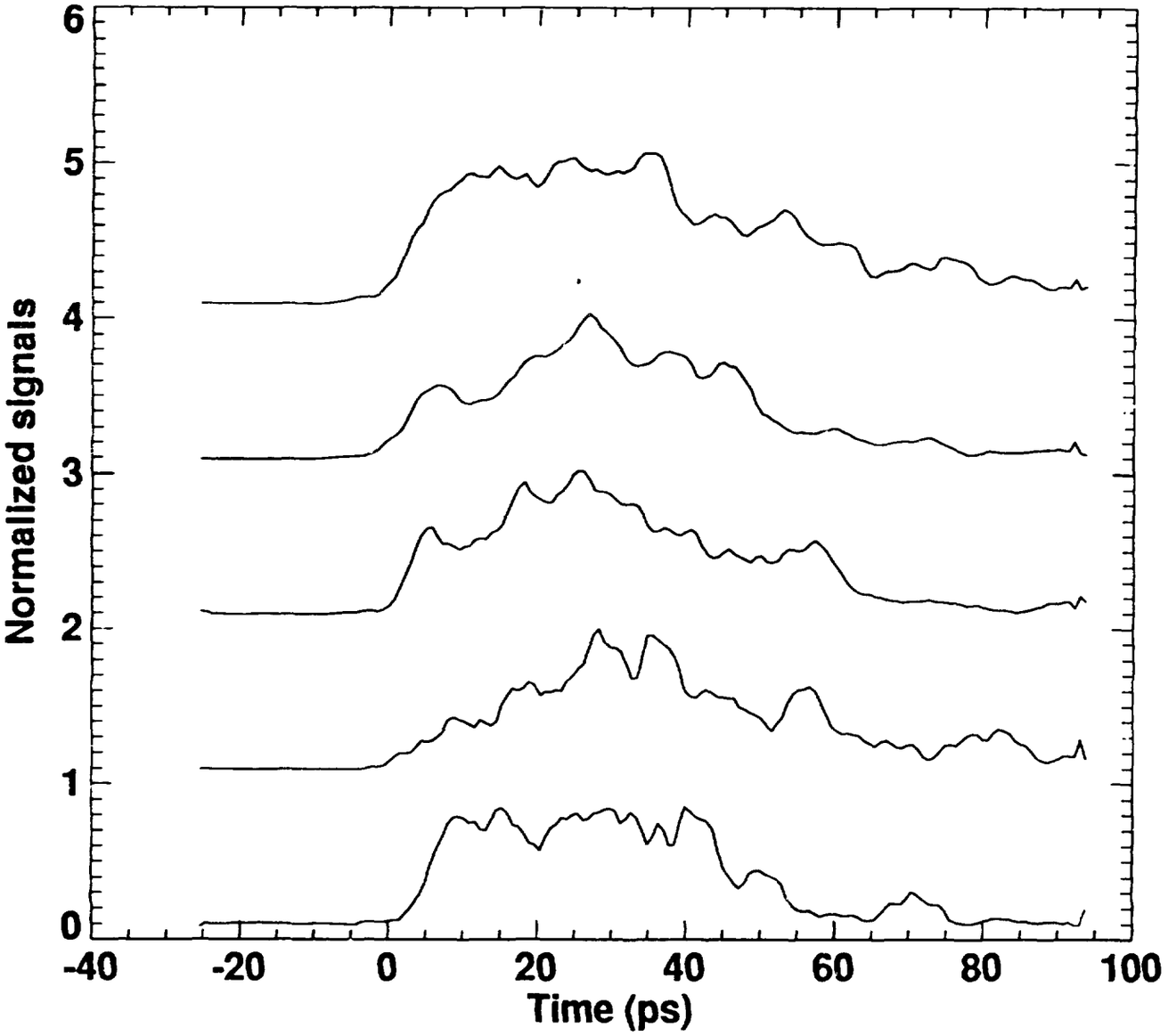
Normalized signals
6
5
4
3
2
1
0
-40
-20
0
20
40
60
80
100
Time (ps)

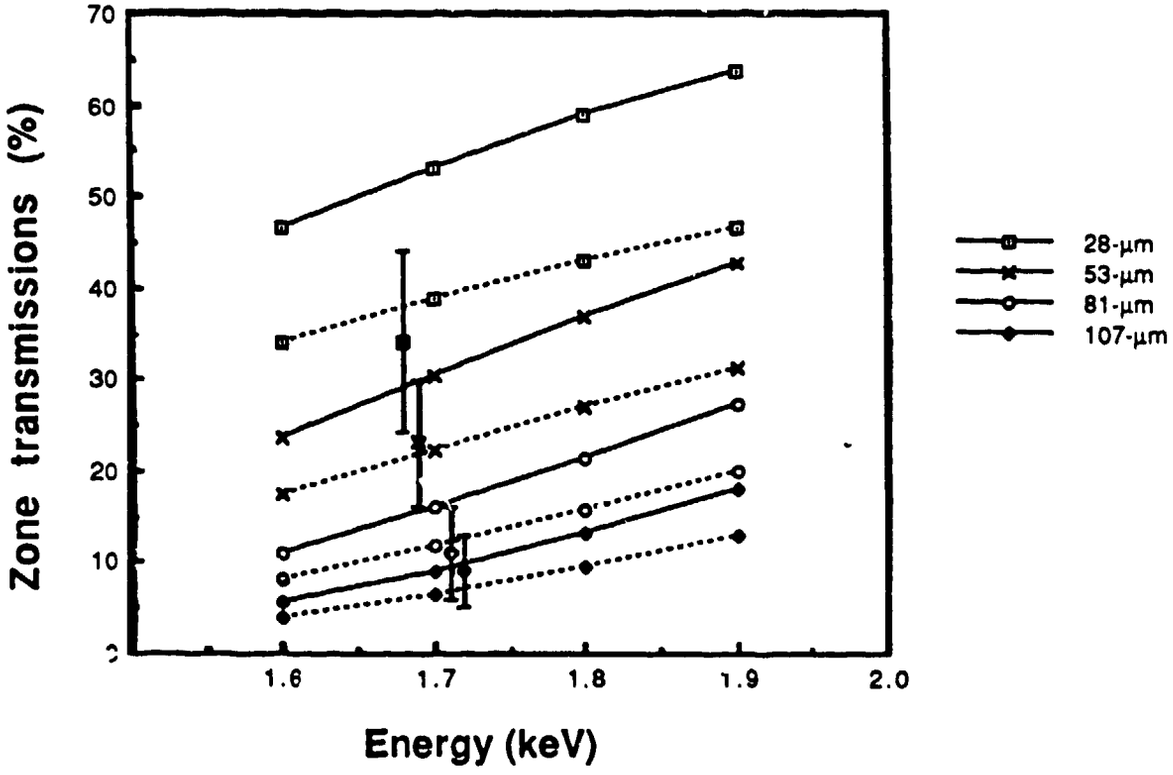
Zone transmissions (%)
70
60
50
40
30
20
10
0
1.6
1.7
1.8
1.9
2.0
Energy (keV)
28-μm
53-μm
81-μm
107-μm

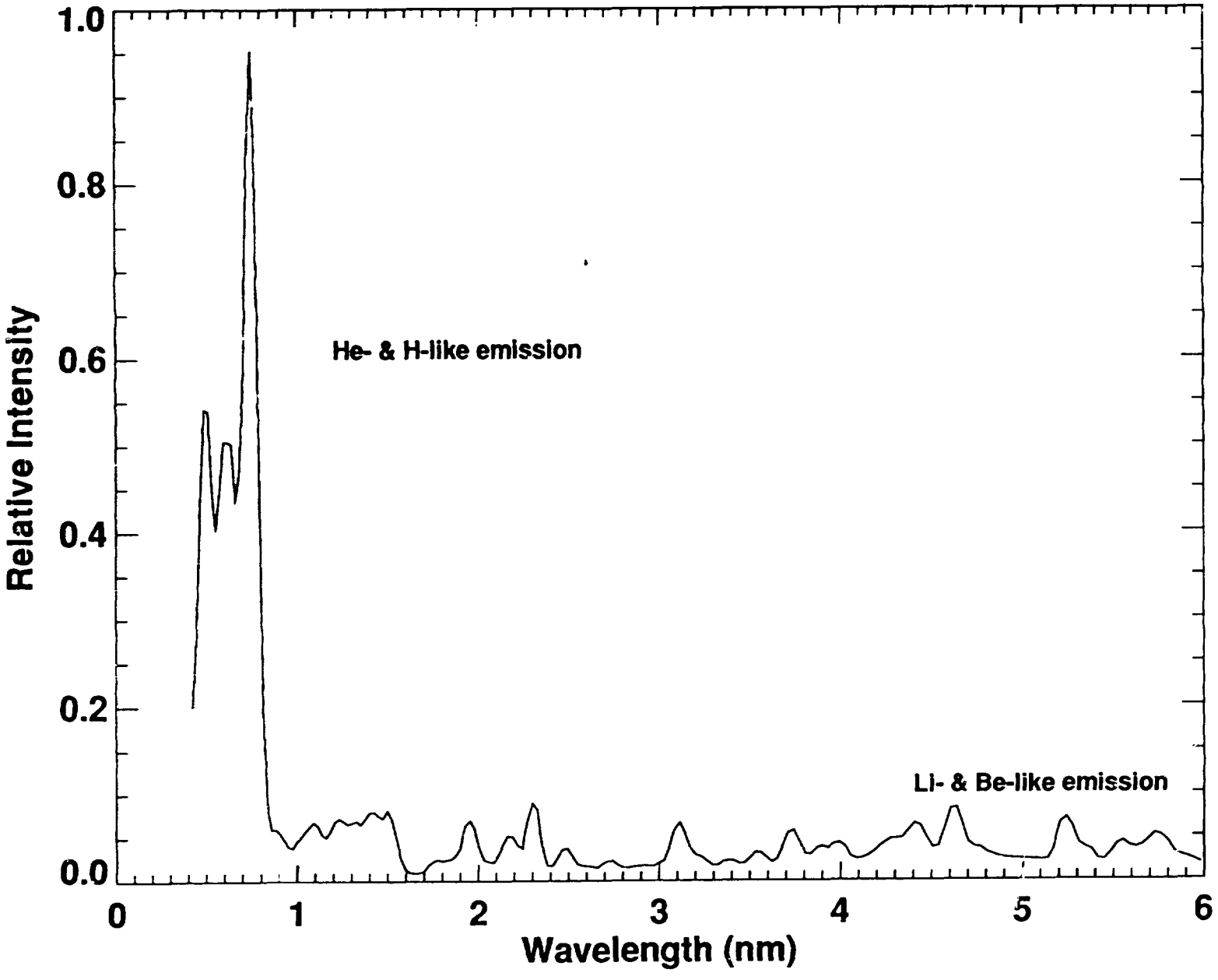
1.0
0.8
0.6
0.4
0.2
0.0
Relative Intensity
He- & H-like emission
Li- & Be-like emission
0
1
2
3
4
5
6
Wavelength (nm)